130 *Chem. Mater.* **2010,** *22,* 130–142
DOI:10.1021/cm902511a

CHEMISTRY OF MATERIALS
Article

Optimizing the Synthesis of Nitrogen-Substituted Zeolites

Karl D. Hammond,[†] Murad Gharibeh,[†] Geoffrey A. Tompsett,[†] Fulya Dogan,[‡] Autumn V. Brown,[§] Clare P. Grey,[‡] Scott M. Auerbach,*[,⊥,†] and Wm. Curtis Conner, Jr.*[,†]

[†]*Department of Chemical Engineering, University of Massachusetts, Amherst, Massachusetts 01003−3110,* [‡]*Department of Chemistry, State University of New York, Stony Brook, New York 11794−3400,* [§]*Department of Chemistry, Gordon College, Wenham, Massachusetts 01984−1813, and* [⊥]*Department of Chemistry, University of Massachusetts, Amherst, Massachusetts 01003−9336*

Received August 15, 2009. Revised Manuscript Received October 20, 2009

We examine the effect of synthesis conditions on the degree of substitution and retention of crystallinity and microporosity during ammonia treatment of Y zeolite. Our objective is to find a reproducibly optimal synthesis protocol to make nitrogen substituted (nitrided) zeolites. We find that a temperature of approximately 750 °C at a mean ammonia flow rate of 600 cm^3/min produces substitution without loss of crystallinity or microporosity. We have investigated the effects of several synthesis parameters using fifteen different synthesis protocols. The most important parameter in the synthesis is the ammonia flow rate; we recommend keeping the flow rate as high as possible. Calculations of the NMR and vibrational spectra of substituted zeolites are used to investigate the overall utility of these techniques for confirming the presence of nitrogen in the zeolite. Infrared and Raman spectroscopy were not found to be diagnostic, but they can corroborate the presence of nitrogen in the framework. We recommend a combination of ^{29}Si MAS NMR spectroscopy, X-ray diffraction, and high-resolution adsorption to test any new reactor design; these techniques can establish nitrogen substitution in the framework, as well as crystallinity and microporosity in the product.

1. Introduction

Zeolites form a class of extremely valuable and important materials that have largely replaced homogeneous acid catalysts in many chemical processes.[1] The subnanometer pores of zeolites provide a unique, confined environment for chemical reactions, often resulting in increased selectivity. There has been growing interest in the last two decades to develop zeolite and other microporous solid catalysts that serve as bases, allowing the selectivity advantages of these materials to be utilized in base-catalyzed reactions.[2−4] Such reactions are particularly important in light of recent interest in biomass conversion reactions, many of which are more active using alkaline catalysts.[5,6]

There are three primary methods of treating zeolites and related materials to induce basic character: (1) ion exchange of sodium or ammonium ions for calcium, magnesium, rubidium, cesium, or barium ions;[7−12] (2) grafting organic bases onto the pore walls, particularly in mesoporous materials;[13−16] and (3) substitution of nitrogen for oxygen (or, similarly, substitution of oxygen for nitrogen in silicon nitride). It is the third type of treatment with which we concern ourselves here.

Substituting nitrogen for oxygen in silica is analogous to substituting an amine for an ether in organic compounds: ethers are generally neutral, whereas amines are basic. Unlike grafting procedures, substitution does not change the effective pore diameter significantly. Nitrogen-substituted zeolites, amorphous silicates, and aluminophosphates are typically prepared by high-temperature treatment of the starting material with ammonia or

*Corresponding author. E-mail: auerbach@chem.umass.edu (S.M.A.); wconner@ecs.umass.edu (W.C.C.).

(1) *Handbook of Zeolite Science and Technology*; Auerbach, S. M., Carrado, K. A., Dutta, P. K., Eds.; Marcel−Dekker: New York, 2003.
(2) Hattori, H. *Chem. Rev.* **1995**, *95*, 537–558.
(3) Barthomeuf, D. *Catal. Rev. Sci. Eng.* **1996**, *38*, 521–612.
(4) Weitkamp, J.; Hunger, M.; Rymsa, U. *Microporous Mesoporous Mater.* **2001**, *48*, 255–270.
(5) Goodwin, J. G., Jr.; Bruce, D. A.; Lotero, E.; Mo, X.; Liu, Y.; Lopez, D. E.; Suwannakarn, K. *Heterogeneous Catalyst Development for Biodiesel Synthesis*; Technical Report; United States Department of Agriculture: Washington, D.C., 2007.
(6) Climent, M. J.; Corma, A.; Hamid, S. B. A.; Iborra, S.; Mifsud, M. *Green Chem.* **2006**, *8*, 524–532.
(7) Corma, A.; Fornés, V.; Martín-Aranda, R. M.; García, H.; Primo, J. *Appl. Catal., A* **1990**, *59*, 237–248.
(8) Rodriguez, I.; Cambon, H.; Brunel, D.; Laspéras, M.; Geneste, P. In *Heterogeneous Catalysis and Fine Chemicals III*; Guisnet, M., Barbier, J., Barrault, J., Bouchoule, C., Duprez, D., Pérot, G., Montassier, C., Eds.; Studies in Surface Science and Catalysis Series; Elsevier: New York, 1993; Vol. 78, pp 623−630.
(9) Wallau, M.; Schuchardt, U. *J. Braz. Chem. Soc.* **1995**, *6*, 393–403.
(10) Ono, Y.; Baba, T. *Catal. Today* **1997**, *38*, 321–337.
(11) Davis, R. J.; Doskocil, E. J.; Bordawekar, S. *Catal. Today* **2000**, *62*, 241–247.
(12) Ono, Y. *J. Catal.* **2003**, *216*, 406–415.
(13) Cauvel, A.; Renard, G.; Brunel, D. *J. Org. Chem.* **1997**, *62*, 749–751.
(14) Zhang, X.; Lai, E. S. M.; Martín-Aranda, R.; Yeung, K. L. *Appl. Catal., A* **2004**, *261*, 109–118.
(15) Regli, L.; Bordiga, S.; Busco, C.; Prestipino, C.; Ugliengo, P.; Zecchina, A.; Lamberti, C. *J. Am. Chem. Soc.* **2007**, *129*, 12131–12140.
(16) Hruby, S. L.; Shanks, B. H. *J. Catal.* **2009**, *263*, 181–188.

 Published on Web 12/04/2009

another amine. Ammonia is by far the most common because of cost and safety concerns, but other alkyl amines such as methyl amine and ethyl amine have been used.[17−19] However, it is extraordinarily difficult to synthesize zeolites with nitrogen substitutions without significant damage to the zeolite framework structure, and published syntheses tend to be difficult to reproduce. Much of this can be attributed to the vast array of synthesis conditions employed in different laboratories throughout the world and the lack of thorough understanding of the sensitivity of the substitution reaction to those conditions. For example, temperature treatment conditions used in the literature vary from as low as 200 °C using alkylamines[17−19] to as high as 1100 °C using ammonia.[20,21] Flow rates are similarly varied: from static conditions (for alkylamines[17−19]) to flow rates of tens,[22−26] hundreds,[20,27] or even thousands[21] of cubic centimeters per minute. A table summarizing the synthesis conditions we have extracted from the literature for crystalline and amorphous silicates and aluminophosphates is available in the Supporting Information. Many of these syntheses are, we suspect, unlikely to produce nitrogen-substituted materials that are structurally similar to their parent materials. In particular, we suspect that any method employing a temperature of less than 500 °C, regardless of the aminating agent, is unlikely to produce substitution because of the strength of the Si−O bond compared to that of the Si−N bond. Batch (nonflow) processes are unlikely to be able to remove water produced by the reaction, as are processes employing low mean fluid velocities. In the present work, we report a reproducible and effective synthesis of nitrided zeolites.

How the resulting materials are characterized is also extremely important. Like the synthesis conditions, the variability in characterization methods so far employed is high. Most characterization relevant to nitrogen-substituted silicates and related materials has been carried out via X-ray diffraction,[18−21] which measures crystallinity; infrared[17,24−28] and Raman spectroscopy, which reveal vibrational characteristics; physical adsorption,[23,24] which gives an estimate of surface area (for non-microporous materials),[29] pore volume, and pore size (especially for mesoporous materials); and nuclear magnetic resonance (NMR) spectroscopy,[18−21,30−38] particularly ^{29}Si magic angle spinning (MAS) NMR for silicates and ^{27}Al and/or ^{31}P MAS NMR for aluminophosphates. We have shown in previous publications[37,38] that the ^{29}Si single-pulse MAS NMR spectrum can be used as an estimate of the extent of reaction (i.e., fractional substitution of oxygen sites) in the zeolite framework. We also demonstrated that the Si/Al ratio and the presence of H^+ versus Na^+ make a significant impact on the final results: the Na form requires higher temperatures and/or longer times to show similar levels of substitution as seen in the comparably treated H-form, and the materials with higher Si/Al ratios (in the acid form, at least) showed higher levels of substitution and stability than high-aluminum Y zeolite.[38] We will now pursue the use of high-resolution adsorption measurements to complete the characterization of nitrided zeolites.

In this article, we investigate the effects of several treatment parameters, considering fifteen different synthesis protocols in all, and make recommendations as to the best synthesis route. In particular, we examine the effects of flow rate of ammonia, treatment temperature, treatment time, and temperature vs time profile on the crystallinity, microporosity, and level of substitution in ammonia treated Y zeolite. We also augment X-ray diffraction and ^{29}Si MAS NMR with high-resolution adsorption (HRADS) isotherms, finding that these three techniques together are crucial for characterizing the nitrided zeolites. These are the primary conclusions of our paper. Furthermore, we investigated whether the use of infrared and Raman spectroscopy—generally much easier, faster, and/or cheaper analyses than either HRADS or NMR spectroscopy—are of significant use in the characterization of amine-treated zeolites. We found that the vibrational spectroscopies are not diagnostic but can corroborate the presence of nitrogen in the zeolite framework.

The rest of this paper describes the synthesis, characterization, and computational methods applied to make and characterize nitrided zeolites (section 2); the results of

(17) Guo, J.; Han, A.-J.; Yu, H.; Dong, J.-P.; He, H.-Y.; Long, Y.-C. *Microporous Mesoporous Mater.* **2006**, *94*, 166–172.
(18) Han, A.-J.; He, H.-Y.; Guo, J.; Yu, H.; Huang, Y.-F.; Long, Y.-C. *Microporous Mesoporous Mater.* **2005**, *79*, 177–184.
(19) Han, A.-J.; Guo, J.; Yu, H.; Zeng, Y.; Huang, Y.-F.; He, H.-Y.; Long, Y.-C. *ChemPhysChem* **2006**, *7*, 607–613.
(20) Zhang, C.-M.; Xu, Z.; Wan, K.-S.; Liu, Q. *Appl. Catal., A* **2004**, *258*, 55–61.
(21) Wakihara, T.; Saito, Y.; Tatami, J.; Komeya, K.; Meguro, T.; Mackenzie, K. J. D.; Takagi, S.; Yokouchi, M. *J. Ceram. Soc. Jpn.* **2008**, *116*, 980–983.
(22) Ernst, S.; Hartmann, M.; Sauerbeck, S.; Bongers, T. *Appl. Catal., A* **2000**, *200*, 117–123.
(23) Narasimharao, K.; Hartmann, M.; Thiel, H. H.; Ernst, S. *Microporous Mesoporous Mater.* **2006**, *90*, 377–383.
(24) Guan, X.; Li, N.; Wu, G.; Chen, J.; Zhang, F.; Guan, N. *J. Mol. Catal. A Chem.* **2006**, *248*, 220–225.
(25) Ernst, S.; Hartmann, M.; Hecht, T.; Jaen, P. C.; Sauerbeck, S. In *Impact of Zeolites and Other Porous Materials on the New Technologies at the Beginning of the New Millennium, Parts A and B*; Aiello, R., Giordano, G., Testa, P., Eds.; Studies in Surface Science and Catalysis Series; Elsevier: New York, 2002; Vol. 142, pp 549−556.
(26) Srasra, M.; Poncelet, G.; Grange, P.; Delsarte, S. In *Molecular Sieves: From Basic Research to Industrial Applications*; Čejka, J., Žilková, N., Nachtigall, P., Eds.; Studies in Surface Science and Catalysis Series; Elsevier: New York, 2005; Vol. 158, pp 1811−1818.
(27) Fink, P.; Datka, J. *J. Chem. Soc., Faraday Trans. 1* **1989**, *85*, 3079–3086.
(28) Kerr, G. T.; Shipman, G. F. *J. Phys. Chem.* **1968**, *72*, 3071–3072.
(29) Brunauer, S.; Emmett, P. H.; Teller, E. *J. Am. Chem. Soc.* **1938**, *60*, 309–319.
(30) Stein, A.; Wehrle, B.; Jansen, M. *Zeolites* **1993**, *13*, 291–298.
(31) Dupree, R.; Lewis, M. H.; Smith, M. E. *J. Am. Chem. Soc.* **1988**, *110*, 1083–1087.
(32) van Weeren, R.; Leone, E. A.; Curran, S.; Klein, L. C.; Danforth, S. C. *J. Am. Ceram. Soc.* **1994**, *77*, 2677–2702.
(33) Impens, N. R. E. N.; Vansant, E. F. *Interface Sci.* **1997**, *5*, 95–101.
(34) Yang, X.; Truitt, R. E. *Zeolites* **1996**, *16*, 249–253.
(35) Xiong, J. M.; Ding, Y. J.; Zhu, H. J.; Yan, L.; Liu, X. M.; Lin, L. W. *J. Phys. Chem. B* **2003**, *107*, 1366–1369.
(36) Maeda, K.; Mito, Y.; Yanagase, T.; Haraguchi, S.; Yamazaki, T.; Suzuki, T. *Chem. Commun.* **2007**, 283–285.
(37) Hammond, K. D.; Dogan, F.; Tompsett, G. A.; Agarwal, V.; Grey, C. P.; Conner, W. C.; Auerbach, S. M. *J. Am. Chem. Soc.* **2008**, *130*, 14912–14913.
(38) Dogan, F.; Hammond, K. D.; Tompsett, G. A.; Huo, H.; Conner, W. C.; Auerbach, S. M.; Grey, C. P. *J. Am. Chem. Soc.* **2009**, *131*, 11062–11079.

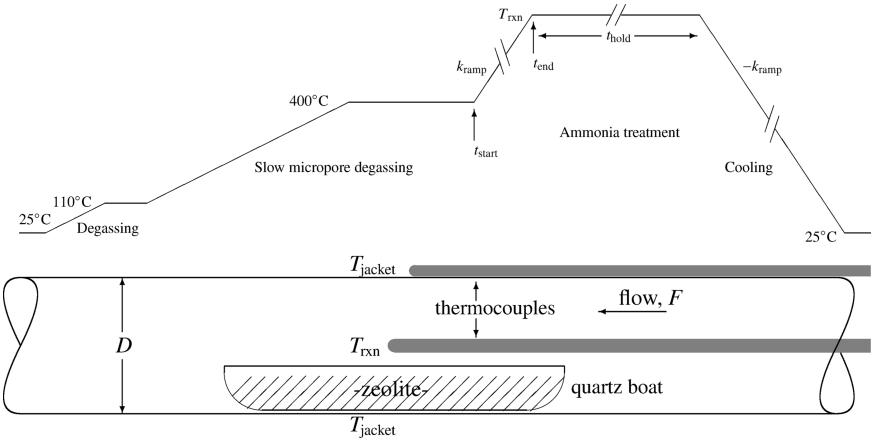

Figure 1. Treatment steps (top) and reactor layout (bottom).

various treatment protocols and the corresponding characterization (section 3); and overall conclusions (section 4). Supporting Information is available online that offers more details regarding past synthesis protocols and present characterization and modeling.

2. Methods

The zeolites analyzed in this article are Y zeolites (FAU framework[39]) with an Si/Al ratio of 6 (Zeolyst Corporation, Valley Forge, PA; product number CBV712, Lot #71200N00868). The zeolite is sold as NH_4Y, which loses ammonia upon heating to form the acidic zeolite HY. The as-sold product is actually more dealuminated than the nominal Si/Al ratio (6) indicates; we find this particular sample to have an apparent framework Si/Al ratio of about 20 based on the NMR spectra (see Figures 4−6).

We note that the Si/Al ratio calculated from the NMR spectrum for the untreated material is about 20 (see Figure 4, for example), obtained via

$$\mathrm{Si/Al} = \sum_{x=0}^{4} I_x / 0.25 \sum_{x=0}^{4} x I_x$$

where I_x is the integral of a peak corresponding to x nearby aluminum atoms. The discrepancy between this value and the manufacturer's value of 6 can be traced to pretreatment conditions: when the zeolite is dealuminated from Si/Al ≈ 2.5 (the Si/Al ratio of the as-synthesized material), to Si/Al ≈ 6 (the Si/Al ratio of the as-sold material), some aluminum remains bound to the material as extra-framework aluminum (EFAl). The combination of EFAl and framework aluminum results in an overall Si/Al = 6, but the ratio estimated by NMR from framework aluminum alone results in Si/Al ≈ 20.

2.1. Treatment. Samples to be substituted with nitrogen were treated by flowing anhydrous ammonia at high temperatures in a fused quartz tube within a tube furnace. The anhydrous ammonia was further dried at room temperature with a glass moisture trap (model SG6191; Advanced Specialty Gas Equipment, Middlesex, NJ), which uses a mixture of NaX and NaA zeolites at room temperature to remove all traces of water. The ammonia renders the cobalt chloride indicator useless, so the desiccant was changed at regular intervals. The temperature was measured with a thermocouple mounted either in the center of the furnace or between the tube and the heater (the "jacket"), with the sample placed in a quartz boat as diagrammed in Figure 1.

Nitrogen-substituted (nitrided) Y zeolite was prepared as follows. Approximately 0.7 g of zeolite were placed in a quartz boat, packed loosely so as to allow rapid removal of water produced by the reaction. This boat was placed in a tube furnace with flowing nitrogen gas and heated at 0.5 °C per minute to 110 °C. This temperature was held for 2 h, and the furnace was then heated at 0.5 °C per minute to 400 °C. That temperature was held for 6 h to ensure the zeolite pores were devoid of water, which is important both to prevent dealumination before ammonia is added and drive the reaction forward after ammonia is added, as the ammonia addition reaction is highly endothermic. The furnace was then heated at k_{ramp} between 1.0 and 1.5 °C per minute to the reaction temperature of 550−850 °C. The gas was changed from nitrogen to ammonia either at the beginning of the ramp (400 °C) or at the end of the ramp after the reaction temperature had been reached (T_{rxn}). The oven was maintained at this temperature for 8−48 h, after which the flow gas was replaced again with nitrogen. The oven was then cooled at the same rate, k_{ramp}, to room temperature. The quartz tube was sealed on both ends with a glass-to-metal (Kovar) seal, which made it possible to seal the thermocouple inside the reactor by threading the thermocouple sheath through the quarter inch fitting. All temperatures were measured by a K-type (chromel-alumel) thermocouple placed inside the tube furnace near the reaction vessel at the center of the furnace ("rxn") or on the outside of the tube furnace next to the heater ("jacket"). A diagram of the treatment steps is included in Figure 1.

There are several process variables given as ranges in the previous paragraph. These are variables involved in the synthesis procedure that can be changed:

- Zeolite sample history (e.g., as-synthesized, dealuminated)
- Charge-compensating cation (H^+/NH_4^+, Na^+)
- Si:Al ratio
- Reactor tube diameter, D
- Center point temperature, T_{rxn}
- Temperature at which ammonia is first introduced, $T_{NH_3} \in \{400\ °C, T_{rxn}\}$
- Volumetric flow rate, F, or, alternatively, the average fluid velocity $4F/\pi D^2$ or the mean Reynolds number Re_D ($\approx 4F/\pi\nu D$ for flow in a pipe)
- Hold time at reaction temperature, t_{hold}
- Ramp rate during final heating step (from 400 °C to T_{rxn}), k_{ramp}
- Temperature control point: either "rxn" or "jacket" as shown in Figure 1.

(39) International Zeolite Association. Database of Zeolite Structures, http://www.iza-structure.org/databases/.

The effects of starting material history, compensating cation, and Si/Al ratio were the subject of our previous publication.[38] In this article, we concentrate on one particular starting material (NH_4Y, Si/Al = 6, dealuminated at the factory to Si/Al ~ 20), and we seek to find one set of reaction conditions that reproducibly gives (a) high crystallinity, comparable to that of the untreated zeolite; (b) reasonably high levels of nitrogen substitution; and (c) micropore volumes comparable to the untreated zeolite. Please see Table 1 for a summary of the synthesis conditions we tested. We can ascertain the effect of changing one synthesis parameter by comparing one or more samples from Table 1. Examples of these are shown in Table 2.

We have not done a full investigation of the effects of tube diameter, but preliminary indications suggest that tube diameter may be a significant parameter. For example, the temperature measured by the probe in the center of the reactor (T_{rxn}) depends strongly on the flow profile, and is sensitive to both heating length and tube diameter. The setup at UMass (D = 2.3 cm, F = 600 cm^3/min) produces $T_{rxn} - T_{jacket}$ on the order of 75−130 °C, whereas the setup at Stony Brook University (D = 3.8 cm, F = 2000 cm^3/min) produces $T_{rxn} - T_{jacket}$ on the order of 5 °C. These differences may be attributable to furnace design and/or tube wall thickness. We therefore emphasize that temperatures should be measured by inserting a thermocouple into the ammonia flow; this ensures that the temperature of the reaction is as close as possible to the reported temperature.

Flow rates were maintained at 70, 600, or 2000 cm^3/min (see Table 1), which were measured using a rotameter. A mass-related factor of 1.3 has been applied to convert from air to ammonia calibration.[40] Kinematic viscosites were calculated using linear extrapolation from the dynamic viscosity measurements of Touloukian et al.[41] and densities given by the ideal gas law (which are very close to the densities measured by Reynolds[42] for lower temperatures). The Reynolds numbers in Table 1 are significantly lower than the value corresponding to the transition to turbulent flow ($Re_D \approx 2300$), indicating that the flow is laminar. After synthesis, all materials were stored under nitrogen inside a sealed vial. Vials were stored in a drybox at less than 25% relative humidity. Moisture conditions in the box were maintained using Drierite (anhydrous calcium sulfate with cobalt chloride indicator; W. A. Hammond Drierite Company, Xenia, OH). Nitrogen gas was ultrahigh purity grade (Airgas East, Salem, NH). Ammonia gas is anhydrous (99.99%; Airgas).

2.2. X-ray Diffraction. X-ray diffraction was measured with a Philips X'Pert Professional diffractometer using a Cu K-α source with a wavelength of 1.54 Å. An accelerating voltage of 45 kV and a current of 40 A were used. A slit width of 0.5° was used on the source. Scans were collected using an X'Celerator detector.

2.3. Physical Adsorption. High-resolution adsorption (HRADS) isotherms were collected with an AUTOSORB−1 MPC (Quantachrome Instruments; Boynton Beach, FL) volumetric adsorption system with a 1 Torr transducer for low pressure readings. Samples were degassed at 300 °C using a turbomolecular pump until the initial differential degassing rate was below 20 μm Hg/min. Points were taken only after the pressure had been stable for 12 min for points below $P/P° = 1 \times 10^{-2}$ and 5 min for all points at higher pressures. The t-plot[43,44] used here employs the universal thickness model of de Boer,[45] which is based on the thickness model of Harkins and Jura.[46] The α_s-plot[47] uses $P/P° = 0.4$ as the point of reference using an isotherm for amorphous, nonporous silica.[48] Micropore volumes were extracted directly from the adsorption isotherms by assuming the density is equal to that of liquid nitrogen (0.001547 cm^3 STP/mL; ref 49.), using the quantity adsorbed at $P/P° = 0.001$. Micropore volumes were also extracted from the t-plot by extrapolating the linear region back to the origin and using that quantity adsorbed as the micropore volume as suggested by Sing.[50] Both micropore assessment techniques require the assumption that the adsorbate density is equal to the liquid density inside the micropores, which is a tenuous assumption at best. As such, all pore volumes should be interpreted relative to other materials, not necessarily as absolute volumes.

2.4. NMR Spectroscopy. Silicon-29 MAS NMR spectra were collected using a Bruker DSX300 spectrometer with a 7.05 T

Table 1. Treatment Conditions (Tr) Used to Test the Effect of Various Process Variables on Final Products[a]

Tr	t_{hold} (h)	F (cm^3/min)	Re_D[b]	T_{NH_3}	T_{rxn} (°C)	T_{jacket} (°C)	k_{ramp} (°C/min)
A	8	70	0.3	820	827	900	1.5
B	8	600	3.3	400	712	829[c]	1.5
C	24	600	3.2	400	730		1.167
D	48	600	3.2	400	730		1.167
E	8	600	2.5	400	850		1.5
F	8	600	2.5	850	850		1.5
G	8	600	3.1	400	750		1.5
H	24	600	2.5	400	850		1.5
I	8	70	0.35	750	750		1.5
J	8	600	3.1	400	750		1.167
K	8	600	3.8	400	650	780	1.5
L	8	600	4.7	400	550		1.5
M	4	600	3.1	400	750		1.5
N[d]	8	600	3.1	400	750		1.5
O[e]	8	2000	5.2	550	845	850	1.5

[a] Symbols are explained in Figure 1, Table 2, and in the text. [b] Note that the Reynolds number also depends on the kinematic viscosity, which is a function of temperature. [c] The temperature for this treatment was controlled using the jacket temperature. [d] Glass wool was placed under the "boat" to ensure minimal thermal contact of the quartz boat with the hot wall. [e] Treatment O was prepared at Stony Brook University using a slightly different furnace with a diameter of 3.8 cm.

Table 2. Parameters Tested for Sensitivity and the Protocols That Demonstrate Their Influence on Reaction Conditions

parameter	symbol	protocols	figure
NH_3 intro. temp.	T_{NH_3}	E, F	3
flow rate	F	A, E, O	4
hold time	t_{hold}	C, D, G, M	5
temperature	T_{rxn}	E, G, K, L	6
ramp rate	k_{ramp}	G, J	N/A
control point	rxn/jacket	B, E	N/A

(40) CK Gas, Inc. Rotameters, Basic Flowmeter Principles, http://www.ckgas.com/html/Rotameters-Basic-Flowmeter-Principles.html.
(41) Touloukian, Y. S.; Saxena, S. C.; Hestermans, P. *Viscosity*; IFI/Plenum: New York, 1975; Vol. 11.
(42) Reynolds, W. C. *Thermodynamic Properties in SI*; Stanford University: Stanford, CA, 1979.
(43) Lippens, B. C.; de Boer, J. H. *J. Catal.* **1965**, *4*, 319–323.
(44) de Boer, J. H.; Linsen, B. G.; Osinga, T. J. *J. Catal.* **1965**, *4*, 643–648.
(45) de Boer, J. H.; Lippens, B. C.; Linsen, B. G.; Broekhoff, J. C. P.; van den Heuvel, A.; Osinga, T. J. *J. Colloid Interface Sci.* **1966**, *21*, 405–414.
(46) Harkins, W. D.; Jura, G. *J. Am. Chem. Soc.* **1944**, *66*, 1366–1373.
(47) Sing, K. S. W. In *Proceedings of the International Symposium on Surface Area Determination*; London, U.K., July 16–18, 1969; Everett, D. H., Ottewill, R. H., Eds.; International Union of Pure and Applied Chemistry: Research Triangle Park, NC, 1970; pp 25–42.
(48) Gregg, S. J.; Sing, K. S. W. *Adsorption, Surface Area, and Porosity*, 2nd ed.; Academic Press: London, 1982.
(49) *AUTOSORB-1 AS1Win Version 1.50 Operating Manual*; Quantachrome Instruments: Boynton Beach, FL, 2004.
(50) Sing, K. S. W. *Chem. Ind.* **1967**, 829–830.

magnet (proton Larmor frequency 300 MHz) using a 4 mm probe. The rotor was spun at the "magic" angle (54.7°) at 3 kHz. Single-pulse experiments were performed with a $\pi/2$ pulse length of 7 μs. Recycle delays of 30, 60, and 90 s showed no change in relative peak heights, so a recycle delay of 30 s was employed in all spectra. Chemical shifts are with respect to tetramethylsilane (TMS) at 0 ppm. All spectra are normalized to have a total integral of unity unless otherwise specified.

2.5. Vibrational Spectroscopy. Infrared spectra were collected with a Bruker Equinox−55 mid-infrared Fourier transform spectrometer. Wavenumbers between 400 cm^{-1} and 4000 cm^{-1} were scanned with 4 cm^{-1} resolution. Samples were prepared as a 1−10% w/w mixture with KBr and compressed at 5000 psig. Fifty scans were averaged to produce the final spectra.

Raman spectra were collected using a HORIBA Jobin Yvon LabRAM Raman microscope using a 50× optical lens, 180° scattering, 632 nm laser line, and 100 μm slits. Ninety 60 s scans were averaged over the range of 100−4000 cm^{-1} to produce each spectrum.

2.6. Calculations. Predicted NMR spectra were generated from chemical shifts calculated using clusters containing 14 tetrahedral (T) atoms using gauge-including atomic orbitals (GIAO),[51,52] the B3LYP hybrid density functional,[53−57] and the cc-pVTZ basis set,[58−63] as implemented in Gaussian.[64] The geometry of each cluster was optimized using the same density functional and the 6-311G(*d*,*p*) basis set.[65,66] The intensity of each peak was estimated by assuming a quasi-random distribution of nitrogen among the various possible substitution sites (≡Si−OH−Al≡ and ≡Si−O−Si≡). The substitution was biased toward Brønsted acid sites according to an adjustable parameter, the bias ratio (BR). The degree of substitution was determined by the fraction of oxygen atoms that must be substituted in order to fit the spectrum. These fitting procedures and the values of all chemical shifts were described in detail in our previous publication.[38]

Predicted vibrational spectra were computed using frequencies derived from the harmonic oscillator approximation using electronic energies calculated using B3LYP/6-311G(*d*,*p*) as implemented in Gaussian.[64] The terminal hydroxide groups were fixed at their crystallographic coordinates during the geometry optimization. During the frequency calculation, the fixed atoms (which are not in a minimum-energy geometry) were given an artificial atomic mass of 10 000 Da, effectively removing the spurious imaginary frequencies that result from the constrained terminal atoms by greatly reducing the intensities of the associated vibrations.

Frequencies higher than 2000 cm^{-1} were scaled by a factor of 0.97; this value was found by Andersson and Uvdal (who published both 0.9619 and 0.9679, recommending the latter),[67] Andrade and co-workers (who published 0.9698 and 0.9678),[68] and Merrick and co-workers (who published 0.9682),[69] to give better agreement with experimental vibrational frequencies. The cutoff of 2000 cm^{-1} is arbitrary; it is unclear from the literature which wavenumbers should be dubbed "high" (and therefore scaled by 0.97) and which should be "low" (and scaled by 1.01 or so), other than the fact that anything above 2000 is clearly relatively high. Cutoffs of 1000 and 1800 cm^{-1} have been used,[69] but typically an exact crossover frequency is not suggested. Frequencies below 2000 cm^{-1} were not scaled, as the "low-frequency" scale factors are essentially unity for B3LYP with the 6-311G(*d*,*p*) basis set.[67−69] The IR and Raman spectra themselves were produced by imposing a Lorentzian line shape on the peak associated with each frequency, multiplying by the calculated intensity of the vibration, and summing over all vibrations. The width (half-width at half-maximum) of the Lorentzian line was 30 cm^{-1} for each vibration for infrared spectra and 5 cm^{-1} for Raman spectra, both of which are adjustable parameters.

Infrared intensities are given by the absorption coefficient, which is directly proportional to the absorbance that would be measured experimentally[70] and has units of m/mol. Calculated Raman intensities are determined from computed scattering activities (*S*, related to the trace of the derivative of the polarizability tensor[71,72]) and parameters from our Raman spectrometer. The differential scattering cross section, which is proportional to the measured intensity, is given by[70]

$$I \propto \frac{d\sigma}{d\Omega} = \frac{\pi^2}{\epsilon_0^2}(\bar{\nu}_i - \bar{\nu})^4 \left(\frac{h}{8\pi^2 c\bar{\nu}}\right)\left(\frac{S}{45}\right)\frac{1}{1-\exp\left(\frac{-hc\bar{\nu}}{kT}\right)} \quad (1)$$

where $\bar{\nu}_i$ is the wavenumber of the exciting beam (1/632 nm = 15800 cm^{-1}), $\bar{\nu}$ is the wavenumber of the Raman transition, T = 300 K, and S is the Raman scattering activity as calculated from the electronic structure calculation. The value of S is calculated in atomic units (Bohr^4/Dalton), and reported in Å^4/Da. Values of S are converted to the appropriate SI units, $C^2\ m^2\ kg^{-1}\ V^{-2}$, by the factor 7.45535×10^{-34} [i.e., $(4\pi\epsilon_0)^2 u^{-1} \times 10^{-40}$ m^4/Å^4, where u is the unified atomic mass unit ($1.66053878 \times 10^{-27}$ kg/Da)]. The differential cross section (eq 1) has units of m^2/sr. Because Raman cross-sections are invariably very small, they are reported in am^2/sr (1×10^{-36} m^2/sr).

3. Results and Discussion

X-ray diffraction is a staple of zeolite characterization. As we have shown in our recent papers on nitrided zeolites,[37,38] silicon-29 MAS NMR is also crucial for

(51) Ditchfield, R. *Mol. Phys.* **1974**, *27*, 789–807.
(52) Wolinski, K.; Hinton, J. F.; Pulay, P. *J. Am. Chem. Soc.* **1990**, *112*, 8251–8260.
(53) Becke, A. D. *Phys. Rev. A* **1988**, *38*, 3098–3100.
(54) Vosko, S. H.; Wilk, L.; Nusair, M. *Can. J. Phys.* **1980**, *58*, 1200–1211.
(55) Lee, C.; Yang, W.; Parr, R. G. *Phys. Rev. B* **1988**, *37*, 785–789.
(56) Stephens, P. J.; Devlin, F. J.; Chabalowski, C. F.; Frisch, M. J. *J. Phys. Chem.* **1994**, *98*, 11623–11627.
(57) Becke, A. D. *J. Chem. Phys.* **1993**, *98*, 5648–5652.
(58) Dunning, T. H., Jr. *J. Chem. Phys.* **1989**, *90*, 1007–1023.
(59) Kendall, R. A.; Dunning, T. H., Jr.; Harrison, R. J. *J. Chem. Phys.* **1992**, *96*, 6796–6806.
(60) Woon, D. E.; Dunning, T. H., Jr. *J. Chem. Phys.* **1993**, *98*, 1358–1371.
(61) Peterson, K. A.; Woon, D. E.; Dunning, T. H., Jr. *J. Chem. Phys.* **1994**, *100*, 7410–7415.
(62) Davidson, E. R. *Chem. Phys. Lett.* **1996**, *260*, 514–518.
(63) EMSL Basis Set Exchange; https://bse.pnl.gov/bse/portal/.
(64) Frisch, M. J.; et al. *Gaussian Development Version, Revision E.X2*; Gaussian, Inc.: Wallingford, CT, 2004.
(65) McLean, A. D.; Chandler, G. S. *J. Chem. Phys.* **1980**, *72*, 5639–5648.
(66) Krishnan, R.; Binkley, J. S.; Seeger, R.; Pople, J. A. *J. Chem. Phys.* **1980**, *72*, 650–654.
(67) Andersson, M. P.; Uvdal, P. *J. Phys. Chem. A* **2005**, *109*, 2937–2941.
(68) Andrade, S. G.; Gonçalves, L. C. S.; Jorge, F. E. *J. Mol. Struct. THEOCHEM* **2008**, *864*, 20–25.
(69) Merrick, J. P.; Moran, D.; Radom, L. *J. Phys. Chem. A* **2007**, *111*, 11683–11700.
(70) Neugebauer, J.; Reiher, M.; Kind, C.; Hess, B. A. *J. Comput. Chem.* **2002**, *23*, 895–910.
(71) Frisch, M. J.; Yamaguchi, Y.; Gaw, J. F.; Schaefer, H. F., III; Binkley, J. S. *J. Chem. Phys.* **1986**, *84*, 531–532.
(72) Gauss, J. Molecular Properties. In *Modern Methods and Algorithms of Quantum Chemistry*; 2nd ed.; Grotendorst, J., Ed.; John von Neumann Institut für Computing: Jülich, Germany, 2000; Vol. 3, pp 541−592.

analyzing these materials. A major finding of this article is that high-resolution adsorption (HRADS) completes the triad of crucial characterization methods for determining the structure and composition resulting from nitridation. To establish this point, we consider a comparison: treatment H to treatment G, which demonstrates both the utility of ^{29}Si MAS NMR spectroscopy and the importance of high-resolution adsorption. This comparison is shown in Figure 2. On the basis of the calculations presented in our previous publications,[37,38] we know that $\delta_{Si} = -88, -67, -62, -51$, and -45 ppm correspond to varying numbers of nitrogen atoms substituted into the zeolite framework. Given the results in Figure 2, this demonstrates that treatment H produces more substitution than treatment G. However, the adsorption isotherms are clearly different: the micropore-filling region (approximately 1×10^{-5} to 1×10^{-3} relative pressure for nitrogen on Y zeolite at 77 K) is well-defined in the untreated material and for treatment G, indicating a well-defined and relatively narrow distribution of pores consistent with Y zeolite. Treatment H has a much broader low-pressure adsorption region and has no definite inflection point, indicating a broad distribution of pores suggestive of a partial collapse of the zeolite structure. The X-ray pattern is reasonably close to that of the untreated material in both cases, though the signal is harder to differentiate from background in the case of treatment H. In addition, the intensities of some of the reflections change after treatment H, which suggests some damage to the crystal structure as well as the micropore structure. Treatment G is therefore a better treatment than treatment H, as it better preserves the pore structure of the zeolite. High-resolution adsorption was crucial in establishing this conclusion.

3.1. Effect of Treatment Conditions. Nearly all treatment conditions from Table 1 result in one or more of the new signals appearing in the ^{29}Si MAS NMR spectrum. However, the amount of substitution (from NMR), degree of crystallinity (from X-ray), and presence and volume of micropores (from adsorption) in the resulting materials depend moderately to highly on the synthesis conditions.

We conducted several syntheses under varied conditions (Table 1) to test the effects of several experimental parameters on the final properties of the material. Samples from each synthesis procedure were analyzed by X-ray diffraction, high-resolution physical adsorption, and ^{29}Si MAS NMR spectroscopy to look for changes in crystallinity, microporosity, and chemical environment (due to substitution), respectively. For the results of these analyses for many of the synthesis protocols we studied, see the Supporting Information. We will concentrate on the comparisons between different protocols (see Table 2) that show the effects of each synthesis variable on the final product.

It should be noted that most treatments result in the broadening and/or disappearance of the Q^3 peak (silicon near one aluminum atom) near -100 ppm. This suggests that Brønsted−Lowry acid sites substitute before Si−O−Si sites, as explored in our previous publications.[37,38]

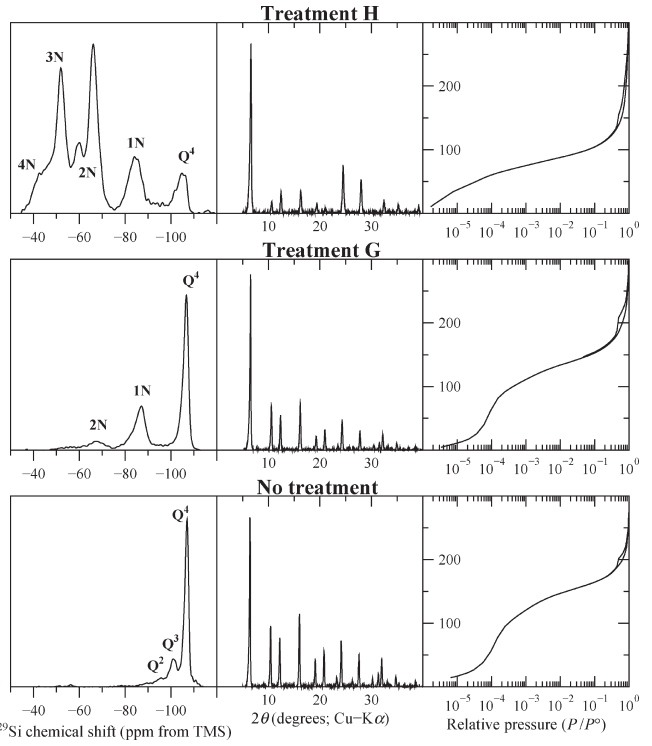

Figure 2. ^{29}Si MAS NMR spectra, X-ray diffraction patterns, and high-resolution nitrogen adsorption isotherms of samples from treatment protocols G and H. The vertical axes for NMR and X-ray plots are in arbitrary units and are autoscaled; for adsorption, the ordinate is in cm^3 STP/g. The differences in the X-ray patterns and adsorption isotherms demonstrate the complementarity of these two methods.

3.1.1. Effect of Ammonia Introduction Temperature/Time. The temperature at which ammonia is introduced to the zeolite seems to be relatively unimportant in terms of the level of substitution, except for the fact that introducing the ammonia before the temperature increases results in a longer time of overall ammonia exposure. However, introducing ammonia before the beginning of the ramp from 400 °C produces ^{29}Si MAS NMR spectra with narrower peaks in the -90 to -100 ppm range, indicating less structural deformation. For example, treatments E and F, which differ only by when ammonia was first introduced, are shown in Figure 3. The high-resolution adsorption isotherms of each material are similar, but there is generally less order evident from the X-ray pattern of material F. The breadth of the NMR peaks indicates the material from treatment F has a larger range of chemical environments than the material from treatment E. This implies that material F probably contains more defects and is less ordered. We suspect that high temperatures in the absence of ammonia cause minor structural deformations as the Si−O and Al−O bonds are thermally excited. When ammonia is present, the same phenomena can also result in substitution in addition to dealumination and/or structural distortion, suggesting that the presence of ammonia either prevents the formation of defects or heals some of them as they form. For this reason, we recommend introducing ammonia before the furnace reaches the reaction temperature, preferably before the zeolite reaches 500 °C.

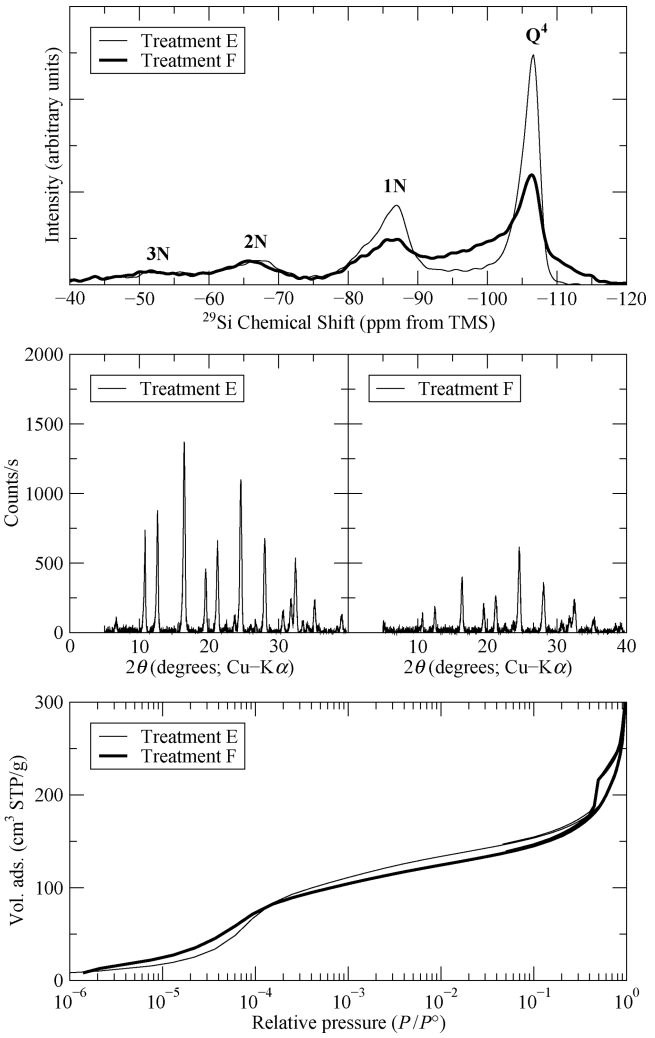

Figure 3. Comparison of the effect of ammonia introduction temperature, T_{NH_3}. The increased intensity for treatment F in the ^{29}Si MAS NMR spectrum between −90 and −100 ppm as well as the shoulder at −110 ppm indicate possible signs of dealumination, defect formation, and other structural changes. Spectra are normalized by sample mass.

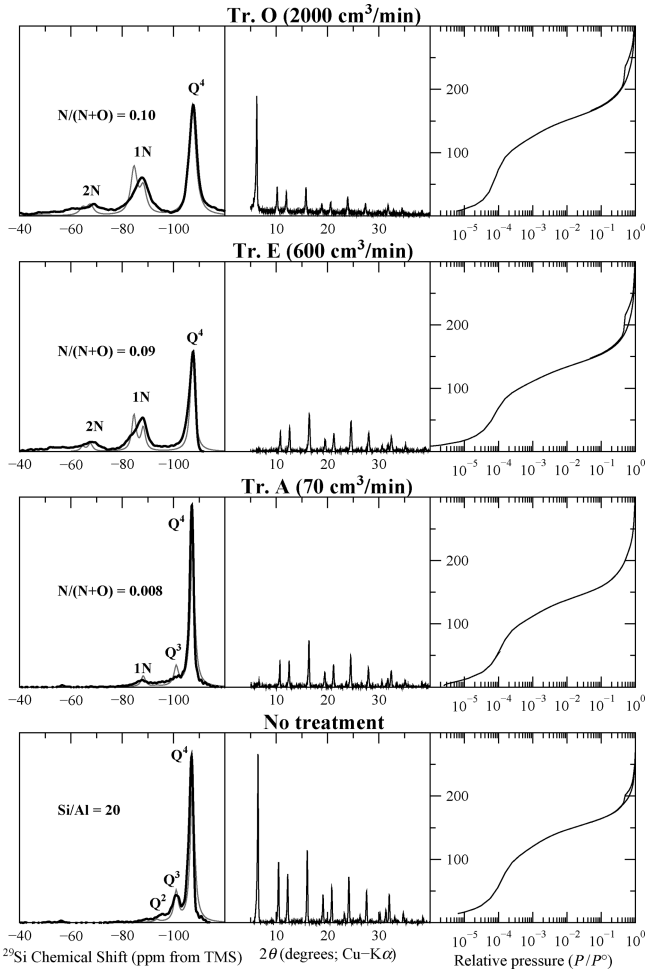

Figure 4. Effect of flow rate on ^{29}Si MAS NMR spectra (left), X-ray diffraction patterns (center), and high-resolution adsorption isotherms (right) at a hold time of 8 h and a temperature of 850 °C. Thick lines are experiment, thin lines are simulations as described in the methods section using the N/(N+O) and Si/Al ratios indicated. Vertical axes are in arbitrary units (NMR, X-ray) and cm^3 STP/g (adsorption). Higher flow rates produce greater substitution and prevent loss of long-range order.

3.1.2. Effect of Flow Rate. Switching from a flow rate of approximately 70 to 600 to 2000 cm^3/min while leaving the temperature at 850 °C and the treatment time at 8 h (from treatment A to E to O in Table 1) produces drastic effects: significantly less nitrogen substitution is evident in the ^{29}Si spectrum (Figure 4) at lower flow rates, whereas the X-ray patterns look much the same except for the low-angle peak near 6.5° and the high-resolution adsorption isotherms are essentially identical to each other and to the untreated sample. In contrast, the higher flow rates (treatments E and O) produce more substitution. This great sensitivity to flow rate suggests that thermodynamic limitations (nitridation is highly endothermic[37,73]) are overcome at higher flow rates by keeping [NH_3] high and [H_2O] low. We recommend 600 cm^3/min as a minimum flow rate; in our configuration, higher values are preferable. The NH_3 flow rate seems to be the most important parameter.

3.1.3. Effect of Treatment Time. The effect of hold time (t_{hold}) is shown for four different values in Figure 5. The effect on the ^{29}Si MAS NMR spectrum is minimal for short times (4−8 h), but at longer times (24−48 h) the bulk of the NMR signal is shifted to less negative chemical shifts, indicating more double and triple nitrogen substitutions. These higher substitutions come at the expense of overall crystallinity and microporosity. Long hold times—especially 48 h—show a marked difference in the high-resolution adsorption isotherm, and a general decrease in micropore volume. These are accompanied by a general decrease in the definition of the signals in the X-ray pattern, suggesting partial collapse of the zeolite structure. The level of substitution seems to be higher at longer times, which is logical, but the general breadth of the peaks in the NMR spectrum also suggests the presence of amorphous (nonzeolitic) material. The degradation of the X-ray pattern is less pronounced at higher flow rates,[38] suggesting that residual water produced by the nitrogen-substitution reaction may dealuminate the zeolite (as would be expected at high temperatures).

(73) Corma, A.; Viruela, P.; Fernández, L. *J. Mol. Catal. A: Chem.* **1998**, *133*, 241–250.

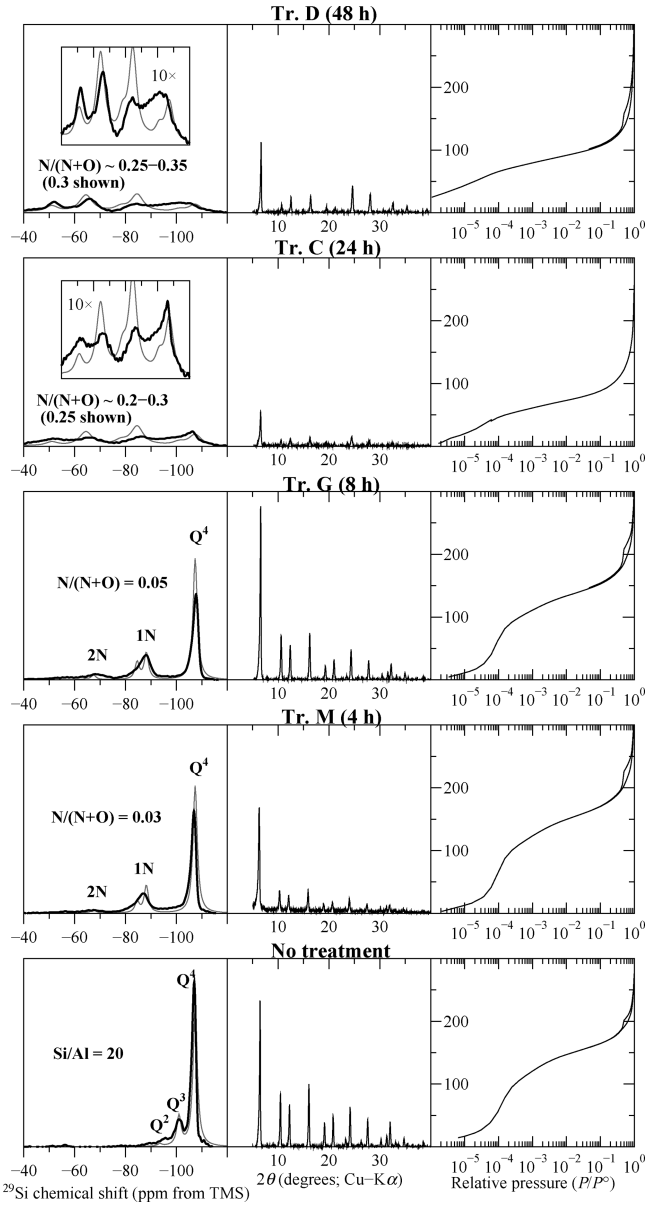

Figure 5. Comparison of ^{29}Si MAS NMR spectra (left), X-ray patterns (center), and high-resolution adsorption isotherms (right) for four different hold times at 750 °C using a flow rate of about 600 cm^3/min. Thick lines (NMR) are experiment; thin lines are the calculated spectra using the N/(N+O) and Si/Al ratios indicated. Longer hold times produce more substitution at the expense of crystallinity and microporosity isotherms, producing an optimum at 8 h for these conditions. Insets: Expanded vertical axis (horizontal axis tick marks are the same).

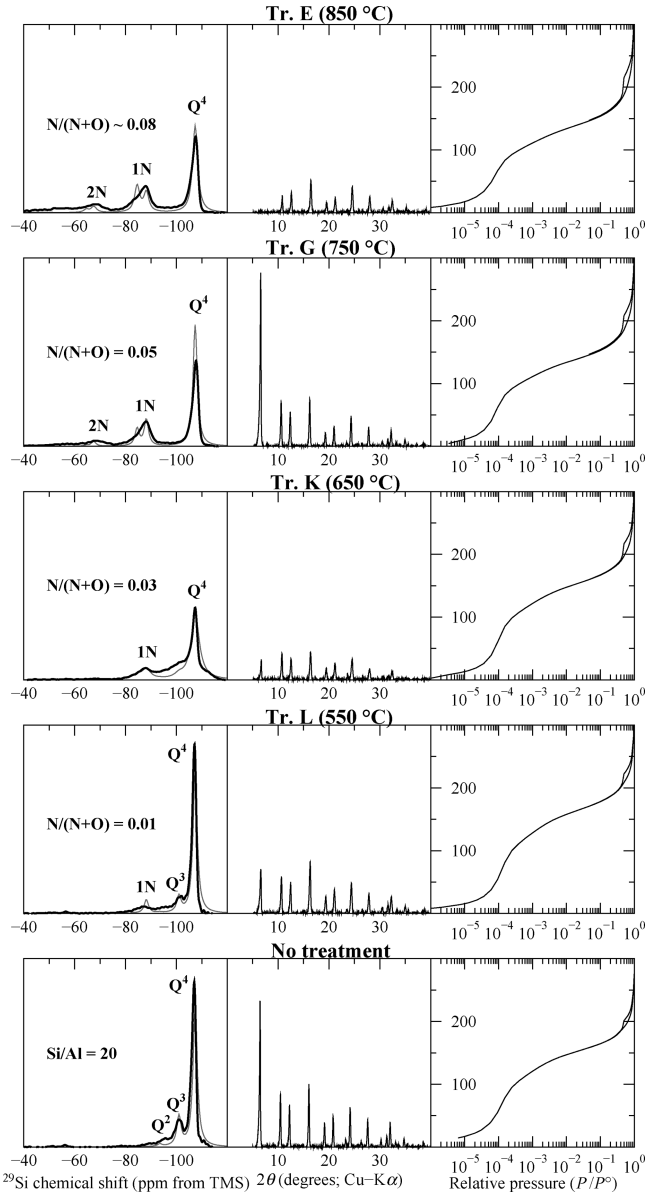

Figure 6. Comparison of ^{29}Si MAS NMR spectra (left), X-ray patterns (center), and high-resolution adsorption isotherms (right) for four different temperatures using an 8 h hold time and a flow rate of about 600 cm^3/min. Thick lines (NMR) are experiment; thin lines are simulations as described in the methods section and ref 38. using the N/(N+O) and Si/Al ratios indicated. Vertical axes are in arbitrary units (NMR, X-ray) and cm^3 STP/g (adsorption).

3.1.4. Effect of Ammonia Treatment Temperature. Increasing the temperature produces more substitution, as seen in the ^{29}Si MAS NMR spectra, leaving the adsorption isotherms more or less unchanged (Figure 6). The X-ray patterns all show peaks in the same places, but with varying intensities. In particular, the first reflection [the (111) face, $2\theta \approx 6.5°$], is diminished after most treatments and completely gone at the highest temperature. However, we suspect the loss of the (111) reflection is due to incomplete removal of ammonia from the zeolite pores before the X-ray pattern was collected, as this peak is very sensitive to the presence of adsorbed species.[74] This is supported by the fact that the peak at low angle reappears after a sample from treatment E had been left sitting under dry nitrogen for several months (see the Supporting Information). This demonstrates that temperatures as high as 850 °C are insufficient to completely destroy the FAU zeolite framework in the absence of water, but also indicates a loss of long-range order. We find that temperatures up to 850 °C produce substituted zeolites with no detectable loss of microporosity.

3.1.5. Recommended Conditions. We are most satisfied with the results of treatment G (8 h, 600 cm^3/min, ammonia started at 400 °C, temperature measured in the center of the reactor, T_{sp} = 750 °C, ramp rate 1.5 °C/min). The X-ray patterns, ^{29}Si MAS NMR spectra, and adsorption

(74) Ciraolo, M. F.; Hanson, J. C.; Norby, P.; Grey, C. P. *J. Phys. Chem. B* **2001**, *105*, 2604–2611.

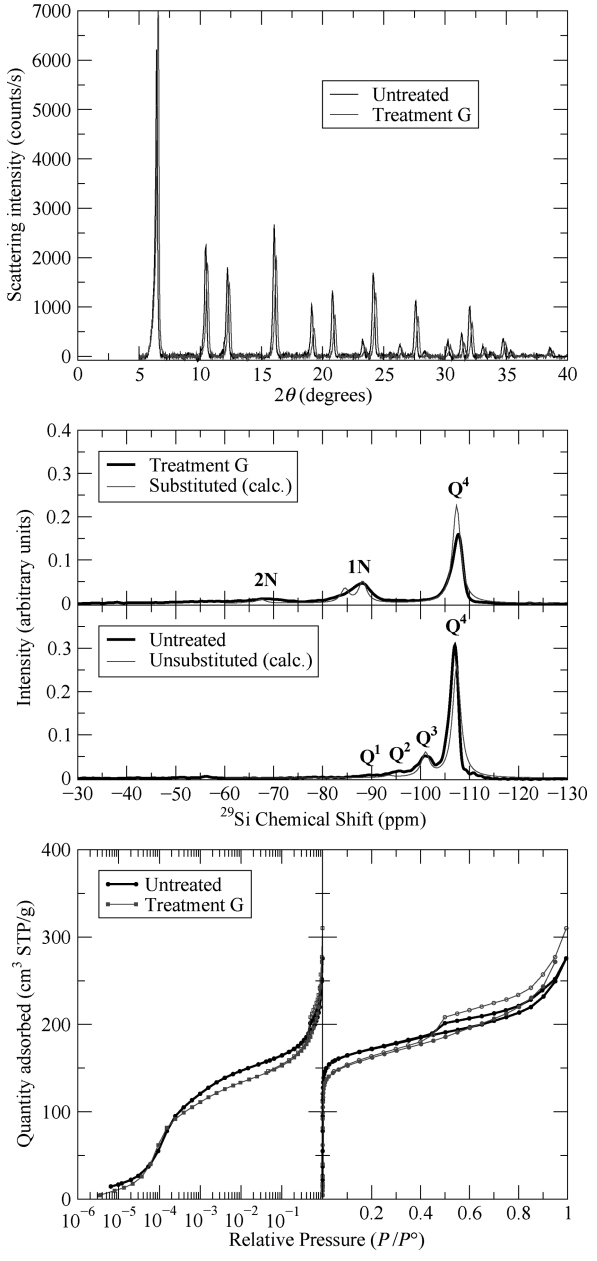

Figure 7. X-ray patterns (top), ^{29}Si MAS NMR spectra (middle), and adsorption isotherms (bottom) of untreated HY zeolite and the same zeolite after treatment G. These results together imply that the material is still crystalline and microporous to the same degree as the starting material, but the NMR spectrum shows nitrogen substitution.

isotherms showing both standard and high-resolution adsorption are shown for treatment G in Figure 7. The three plots in Figure 7 demonstrate to our satisfaction that we have produced nitrogen-substituted Y zeolite that is crystalline and highly microporous. The fit from our calculations supports the conclusion that the zeolite framework remains intact, and indicates that most substitutions occur between silicon and aluminum atoms. We have repeated treatment G at UMass twice, producing essentially identical results (see the Supporting Information). We also ran a similar synthesis using twice as much material distributed back-to-back in two boats; the results are similar to that using only one boat, showing only a slight decrease in the extent of substitution.

3.2. Vibrational Spectra. Vibrational spectroscopy is commonly used to study nitrided silica, zeolites, and aluminophosphates.[17,24−28] As such, we performed vibrational spectroscopy simulations and experiments in an effort to determine the utility of these methods for characterizing nitrided zeolites. The experiments focus on treatment G from Table 1, which we chose primarily because it has the least-changed X-ray pattern and adsorption isotherm but still shows substitution. These results supplement our earlier findings in the NMR spectrum,[38] which suggested ^{29}Si MAS NMR can be used as a measure of the degree of substitution.

Although NMR spectroscopy, discussed with respect to nitrogen substituted zeolites in ref 38, is a local probe specific to one nucleus, vibrational spectroscopy involves the coupled motions of several nuclei at the same time. It is therefore impractical to calculate a "composite" infrared/Raman spectrum by summing over the vibrations around each nucleus, as we have done previously to produce ^{29}Si MAS NMR spectra.[38] Instead, we are forced to compare changes in the spectrum of a single cluster because of the replacement of one oxygen atom with nitrogen. We performed a convergence study on various sized clusters (5, 7, 8, 10, and 14 tetrahedral atoms) clipped from the SOD framework (structurally similar, but not identical, to the FAU framework[39]), which indicates that clusters of at least eight tetrahedral atoms are required to obtain frequencies converged to within about 5 cm^{-1} due to system size considerations. The results of these studies are included in the Supporting Information.

We show a comparison of the IR spectra due to substitution at a siliceous site (Si−O−Si) and an acid site (Si−OH−Al) in Figure 8, using the same cluster employed in our prior publication.[38] The cluster contains 14 tetrahedral atoms, with the vibrations in question at least two or three bond lengths away from the edges of the cluster. The only substantial changes are the Si−N−Si stretching modes, which are only slightly shifted from the corresponding stretching modes of Si−O−Si groups, and the N−H stretching and bending modes. In particular, the shift in the Si−O−Si stretching modes near 1100 cm^{-1} suggests that the observed peak at 969 cm^{-1} (in the difference spectrum) is indeed the Si−N−Si stretching mode, which appears at approximately 989 cm^{-1} in the calculated spectra. A table of these changes for the 5−14 tetrahedral atom clusters mentioned in the previous paragraph is included as Supporting Information. It should be noted that even a cluster containing 14 tetrahedral (T) atoms is too small to capture the "ring-breathing" vibration near 620 cm^{-1}; this vibration involves too many atoms simultaneously to be seen in a cluster of anything close to this size.

Changes in the Raman spectra are similarly subtle. A comparison of treated and untreated Raman spectra, as well as a comparison of substituted clusters' Raman spectra with unsubstituted clusters, is shown in Figure 9 using the same materials and clusters used for the IR spectra in Figure 8. It should be noted that vibrations

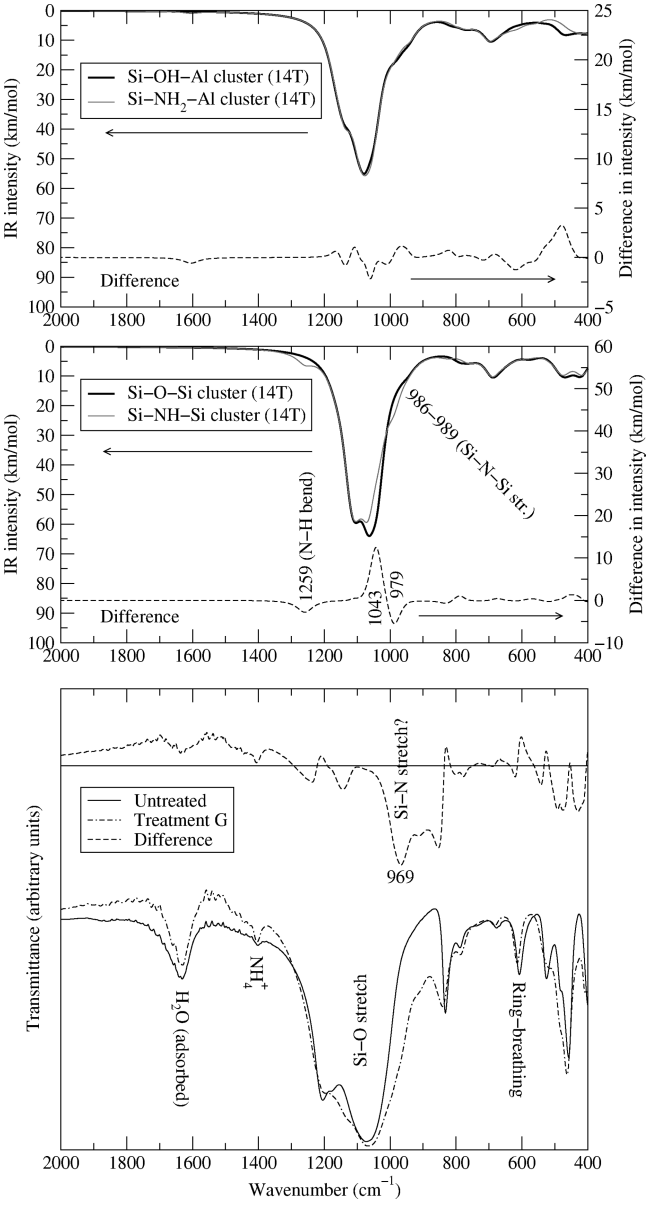

Figure 8. Comparison of the changes in the infrared spectrum of a cluster with a substitution at an acid site (top) and a siliceous site (middle). The bottom graph shows a comparison of the infrared spectra for untreated HY zeolite and the results of treatment G from Table 1 (750 °C, 8 h, 600 cm^3/min, ammonia introduced at start of ramp).

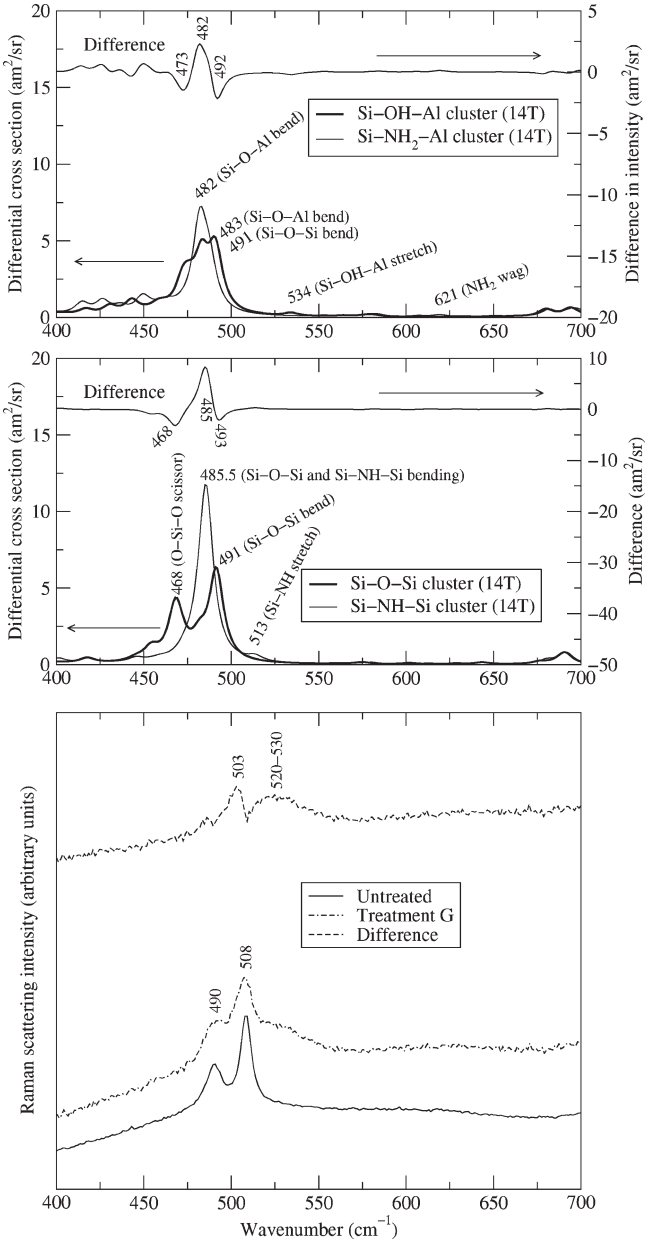

Figure 9. Comparison of the changes in the Raman spectrum of a cluster with a substitution at an acid site (top) and a siliceous site (middle). The bottom graph shows a comparison of the infrared spectra for untreated HY zeolite and the results of treatment G from Table 1 (750 °C, 8 h, 600 cm^3/min, ammonia introduced at start of ramp).

above approximately 750 cm^{-1} are not visible in the final spectrum because of fluorescence; as such, we examine only the region below 700 cm^{-1} in the figures. The only significant difference between the Raman bands of substituted and unsubstituted clusters is the diminishment of the two bands at 468 and 491 cm^{-1} and the enhancement of the band at 482−485 cm^{-1} in both siliceous and aluminum-containing clusters. These bands correspond to Si−O−Si and Si−NH−Si bending modes (see Figure 8). Although it is hardly diagnostic, it is fair to say that the broadening of the two resonances near 500 cm^{-1} in the experimental Raman spectrum is consistent with the trends in the cluster calculations due to nitrogen substitution.

Comparison of the treated and untreated vibrational spectra in Figures 8 and 9 strongly suggests that there is no obvious diagnostic band characteristic of Si−N−Si or Si−N−Al vibration that presents itself after the nitrogen substitution reaction. However, we have not yet looked at the high-frequency vibrations, which are characteristic of N−H and O−H stretching. Calculated IR and Raman spectra in this region are shown in Figure 10. The order of the N−H stretching peaks is O−H > $\nu_{as}NH_2$ (surface) > ν_sNH_2 (surface) > N−H > $\nu_{as}NH_2$ (Si−NH_2−Al) > ν_sNH_2 (Si−NH_2−Al). This partially agrees with the initial assignments of Ernst and co-workers.[25] Our results indicate that the peak they assign to ν_sNH_2 (3441 cm^{-1}) should probably be assigned to $\nu_{as}NH_2$, whereas the shoulder at 3390−3400 cm^{-1} should be assigned to a combination of ν_sNH_2 and

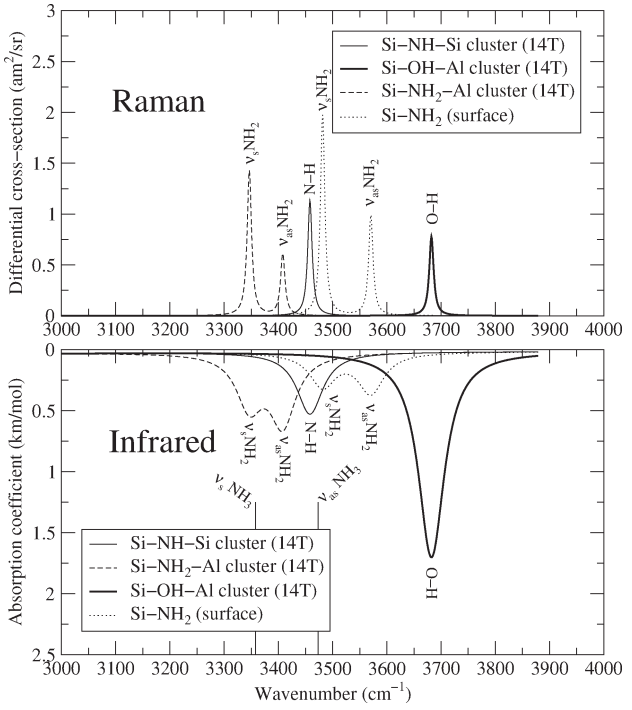

Figure 10. Predicted infrared and Raman spectra at high frequencies for clusters containing Si−NH−Si, Si−OH−Al, and Si−NH_2−Al groups. The hash marks above the legend are the calculated locations of the stretching modes of the ammonia molecule. All frequencies have been scaled by 0.97.

Si−NH−Si. We include a table of experimental and calculated vibrational frequencies in the Supporting Information.

The predicted and measured infrared and Raman spectra suggest that vibrational spectroscopy may provide corroborating evidence of N−H and Si−N/Al−N bond formation, but the peaks are indistinct from those normally evident in the untreated zeolite and/or from ammonia adsorbed on a zeolite. As such, vibrational spectroscopy does not provide any diagnostic test for nitrogen substitution. We therefore recommend the use of IR/Raman as supplementary analysis only—they are not in themselves confirmation of nitrogen substitution for oxygen in the zeolite framework.

3.3. Adsorption Isotherms. There are two regions of the adsorption isotherm that are of relevance: the "standard" region (usually viewed with the abscissa in units proportional to pressure, as shown in the bottom right pane of Figure 7) and the "high-resolution" region (usually viewed with the abscissa in units proportional to the logarithm of pressure, as shown in the lower left pane of Figure 7 and in all other figures showing adsorption isotherms). The logarithmic axis allows one to see the region of the adsorption isotherm in which micropores fill. Unfortunately, high-resolution adsorption requires specialized equipment and is therefore unavailable on many instruments.

Techniques exist that attempt to use information from the standard region of the adsorption isotherm to gain information about the volume of the micropores.[48,75] The α_s plot of Sing[47] and the *t*-plot method of de Boer,[43,44] in particular, have been suggested. Both of these methods involve extrapolation of the nonporous region of the isotherm to the limit of zero pressure; the intercept is related to the volume of the micropores. Although the assumption of liquid density to calculate actual volumes (as suggested by Sing[50]) is not perfect because of compression of the adsorbate as the pressure rises, it is extremely common practice and a reasonable starting point.

Table 3. Comparison of Micropore Volumes Determined from the *t*-Plot, α_s-Plot, and Extrapolation of the Quantity Adsorbed at $P/P^\circ = 0.001$ for the treatment protocols in Table 1[a]

	$V_{\mu p}$ (mL/g)			
Tr	*t*-plot	α_s-plot	$P/P^\circ = 0.001$	N/(N + O)
none	0.2071	0.1904	0.1870	0
A	0.1669	0.1402	0.1738	0.008
B	0.04790	0.03183	0.06653	
C	0.07034	0.04824	0.09477	~0.25
D	0.1041	0.0840	0.1234	~0.3
E	0.1710	0.1486	0.1722	0.09
F	0.1437	0.1170	0.1619	
G	0.1726	0.1512	0.1722	0.05
H	0.09375	0.07127	0.1166	
K	0.2008	0.1814	0.1887	0.03
L	0.2198	0.2005	0.1990	0.01
M	0.2002	0.1788	0.1912	0.03
N	0.2012	0.1798	0.1956	
O	0.1949	0.1703	0.1947	0.09−0.1

[a] N/(N + O) ratios are approximate and determined from fits to the ^{29}Si MAS NMR spectra.

We include a comparison of micropore volumes as determined by the *t*-plot method using the universal thickness model of de Boer,[45,46] the α_s method[47] using amorphous silica[48] as the reference isotherm, and the volume of micropores as estimated from the quantity adsorbed at $P/P^\circ = 1 \times 10^{-3}$ assuming liquid density (0.00154 cm^3 STP/mL) in Table 3. As can be seen from Table 3, the values of the micropore volume disagree by as much as 50% using the *t*-plot/α_{ss}-plot methods and the volume adsorbed at 0.001 relative pressure. In each case where there is significant deviation, there is a visually distinct change in the high-resolution region of the adsorption isotherm as well as a significant drop in the micropore volume—compare, for example, treatment D to the untreated material (Figure 5). As such, it is reasonable to conclude that the isotherm has not changed significantly—and thus the micropore volume is effectively unchanged—if the micropore volume of the treated material (from the *t*/α_s-plots or from the quantity adsorbed at 0.001) is not significantly lower (say, within 15%) than the micropore volume of the untreated material.

One further adsorption-related topic deserves additional discussion. Many authors attempt to make use of the BET surface area, determined from the equation of Brunauer, Emmett, and Teller,[29] for zeolites. This equation makes the assumption that no pores fill in or below the region of the isotherm where the equation is being applied (typically 0.1−0.3 relative pressure), which is obviously an incorrect assumption for zeolites and other

(75) Rouquerol, F.; Rouquerol, J.; Sing, K. S. W. *Adsorption by Powders and Porous Solids*; Academic Press: San Diego, 1999.

microporous materials such as metal-organic frameworks (MOF's). In general, the second fitting parameter in the BET equation, usually designated C_{BET} or simply C, should be in the range 50−150[48] or 50−200[75] to "trust" the BET surface area. For zeolites, including the materials studied in this article (see Supporting Information), C is often negative or extraordinarily large (~6000). As such, we recommend avoiding discussions of "BET surface areas" of zeolites and instead concentrating on high-resolution adsorption. If high-resolution equipment is unavailable, careful comparison of the micropore volumes determined from the t- or α_s-plots with those obtained for the untreated material is a reasonable substitute.

Our overall recommendation is to use a combination of ^{29}Si MAS NMR, X-ray diffraction, and high-resolution physical adsorption to analyze nitrogen-substituted zeolites and related materials. We find that an optimum temperature of approximately 750 °C with a volumetric flow rate of 600 cm^3/min for 8 h produces substitution without loss of crystallinity or microporosity. The most important parameter in the synthesis is the ammonia flow rate, which is intimately linked with the steam removal rate—the flow rate should be higher than approximately 600 cm^3/min for tube diameters similar to our 2.3 cm reactor, suggesting a minimum mean fluid velocity of $4F/\pi D^2 = 145$ cm/min.

4. Conclusions

We have examined the effect of synthesis conditions on the degree of substitution and retention of crystallinity and microporosity during ammonia treatment of Y zeolite. We have found an optimum temperature for the flow rates considered that produces crystalline materials with high microporosity that shows appreciable nitridation. A relatively high flow rate of ammonia is crucial for maintaining crystallinity and microporosity, however, suggesting that the presence of ammonia or the absence of water (which is produced by the reaction) heals defects and/or prevents them from causing dealumination.

For our reactor, the following procedure appears optimal: ammonia introduced before the reactor reaches 500 °C, a hold temperature of 750 °C, and hold times of about eight hours. Introducing ammonia at 850 °C (treatment F in Table 1) causes what appears to be competition between substitution and dealumination reactions, and significant dealumination occurs before the ammonia reaction starts. Longer hold times produce distortions of the zeolite pores, which manifest as changes in the X-ray pattern and decreases in the amount adsorbed in the high resolution adsorption isotherms (Figure 5). Higher temperatures produce slightly higher levels of substitution and minimal changes in crystallinity or microporosity.

Every characterization method has the potential to yield useful information about these materials, but we have found some to be more useful than others. Silicon-29 MAS NMR is a critical analysis to perform if one wants an indication of the number of nitrogen substitutions in the zeolite framework. X-ray diffraction is the only test for crystallinity, but as can be seen from Figure 5, nitrogen substitution for as little as 4 h can decrease the intensity of X-ray peaks severely, even though the micropores remain intact. High-resolution adsorption is also a very important analysis for working with these materials, and yields valuable information about any distortions of the zeolite pores that have occurred. If such equipment is unavailable, a crude substitute can be made via comparison of the micropore volumes calculated from an α_s plot, a t-plot, or the quantity adsorbed at $P/P^\circ = 1 \times 10^{-3}$ (for FAU zeolites; materials with different sized pores will require a different value of P/P°) with the micropore volume of the untreated material.

Our predicted and measured infrared and Raman spectra suggest that vibrational spectroscopy may provide corroborating evidence of N−H and Si−N/Al−N bond formation, but it is not in itself confirmation of nitrogen substitution for oxygen in the zeolite framework because of overlapping bands. We therefore recommend the use of IR and Raman as supplementary analyses only.

We recommend testing any synthesis procedure designed to produce nitrogen-doped zeolites—indeed, any modification of a zeolite framework—using a combination of ^{29}Si MAS NMR spectroscopy, X-ray diffraction, and high-resolution adsorption to ensure the resulting materials are indeed substituted with nitrogen and remain highly crystalline and microporous.

Acknowledgment. We thank Dr. Weiguo Hu and the UMass NMR facility for NMR experiments, Dr. Wim de Jeu of UMass Polymer Science and the UMass X-ray facility for X-ray experiments, Professor Shaw Ling Hsu of UMass Polymer Science for use of the Raman spectrometer, and Tim Landers at UMass for glassblowing. This research was generously funded by the National Science Foundation (CBET-0553577 and REU-0649134) and the United States Department of Energy (DE-FG02-07ER15918 and DE-FG02-96ER14681).

Nomenclature

$\bar{\nu}$	Wavenumber of IR/Raman transition
$\bar{\nu}_i$	Wavenumber of Raman excitation source
ϵ_0	Electric constant
Ω	Solid angle
σ	Cross-section
c	Speed of light
D	Tube furnace inner diameter
F	Volumetric flow rate of ammonia
h	Planck's constant
I	Intensity
k	Boltzmann's constant
k_{ramp}	Heating rate between 400 °C step and final reaction temperature, in °C/min
P°	Saturation pressure
P	Pressure
Re_D	Mean Reynolds number, $\bar{u}D/\nu = 4F/\pi\nu D$, for flow in a pipe
S	Raman scattering activity; this quantity is what is computed in an electronic structure calculation

T	Absolute temperature.
t_{hold}	Time the reaction is maintained at the highest temperature before ammonia is discontinued and the sample is cooled.
T_{NH_3}	Temperature at which ammonia is introduced. In this study, this was between 400 °C and T_{rxn}
T_{sp}	Temperature set point
T_{rxn}	Temperature (°C) at the center of the tube furnace, as measured by a K-type thermocouple mounted there.

Supporting Information Available: Full list of previously published synthesis parameters used by other authors; X-ray patterns, ^{29}Si NMR spectra (single pulse and ^{1}H/^{29}Si cross-polarization), and high-resolution nitrogen adsorption isotherms including *t*-plot, α_s-plot, and BET plot information for most of the treatment procedures in Table 1; convergence information for FAU/SOD vibrations; vibration band positions for nitrided zeolites (this work and literature assignments); and the full citation for ref 64 (PDF). This material is available free of charge via the Internet at http://pubs.acs.org.